AN ABSTRACT OF THE THESIS OF

Marina Marcelli for the degree of Master of Science in Geology presented on November 20, 2020.

Title: The Effects of Structure and Volcanic Stratigraphy on Groundwater and Surface Water Flow: the Hat Creek basin Case Study, California, USA

Abstract approved: _____

Andrew J. Meigs

Hydrogeologic systems in the southern Cascade Range develop in volcanic rocks where volcanic morphology, stratigraphy, extensional structures and attendant basin geometry play a central role in groundwater-flow paths, groundwater/surface-water interactions, and spring discharge locations. High-volume springs (> 3 m^3/s) flow from young (< 1 Ma) volcanic rocks in the Hat Creek and Fall River tributaries, contribute approximately half of the average annual flow of the Pit River, the largest tributary to Lake Shasta and the Sacramento River. We build a hydrogeologic conceptual framework for the Hat Creek basin that combines new geologic mapping, water-well lithologic logs, lidar mapping of faults and volcanic landforms, streamflow measurements, and an aerial stream-temperature survey (Thermal InfraRed; TIR). Data from geologic maps, well logs and lidar are used to integrate the geologic structure and the volcanic and volcaniclastic stratigraphy in the basin. Streamflow measurements and TIR estimates of stream-temperature allow for identification of locations of likely groundwater/surface-water interactions. Two large streamflow gains suggest focused groundwater input to Hat Creek near Big Springs and north of Sugarloaf Peak. These large inflows likely result from geologic groundwater-flow impediments that restrict lateral groundwater-flow and force water into the creek. The inferred groundwater-flow barriers divide the aquifer system into at least three compartments. The two downstream compartments lose streamflow in the upstream sections (immediately downstream of the groundwater-flow impediments) and gain in downstream sections.

Marina Marcelli
November 20, 2020

The Effects of Structure and Volcanic Stratigraphy on Groundwater and Surface Water Flow: the Hat Creek basin Case Study, California, USA

by
Marina Marcelli

A THESIS

submitted to

Oregon State University

in partial fulfillment of
the requirements for the
degree of

Master of Science

Presented November 20, 2020
Commencement June 2021

Master of Science thesis of Marina Marcelli presented on November 20, 2020

APPROVED:

Major Professor, representing Geology

Dean of the College of Earth, Ocean, and Atmospheric Sciences

Dean of the Graduate School

I understand that my thesis will become part of the permanent collection of Oregon State University libraries. My signature below authorizes release of my thesis to any reader upon request.

Marina Marcelli, Author

ACKNOWLEDGEMENTS

I would like to express sincere appreciation to everyone who helped and supported me during this process. A proper list, conveying everything, would be as long as this thesis. I will be brief.

Most people have the privilege of working with one adviser, I was lucky enough to have two. First, thanks to Andrew Meigs and Erick Burns for ushering me through this process, even when I seemed determined to unintentionally shoot myself in the foot. In particular, thanks to Andrew Meigs who began advising me when I was an over-ambitious undergraduate and continued, probably despite his better judgment, to work with me through this master's degree. As for Erick, thank you for making this opportunity available to me, for being a thoughtful and deft scientific role model, and for eloquently guiding me towards becoming a better, more coherent scientist.

Thanks to Patrick Muffler, Jennifer Curtis, Christian Torgersen, Drew Downs and all the others at USGS who took time out of their day to help me in the field or to understand the datasets I've been using (of which there are many).

Thanks to Danielle Woodring and the ladies of lab 204, whose senses of humor, good advice, and geologic know-how continue to help me through the anxieties of an early career scientist. It's not just what I've learned in the field or the classroom, but beyond that too, you guys have changed my life.

Finally, thanks to my family. Thanks to Marco and Lisa Marcelli, for helping, loving and encouraging me, even when they had no idea what I was doing. Thanks to my brother, Lucas, for his good advice and terrible sense of humor. Thanks to my cousins, Devin and Michael and my uncle and aunt, Dave and Ming Li.

I owe all of you so much and scarcely know how to convey it. So please accept my gratitude and sincerest thanks.

TABLE OF CONTENTS

TABLE OF CONTENTS (Continued)

Page

LIST OF FIGURES

LIST OF TABLES

LIST OF EQUATIONS

1 Introduction

The Cascade Range is a primary control on water resources in the Pacific Northwest, USA, dividing the wet western parts of Oregon, Washington, and northern California from the semi-arid east. Precipitation in the Cascade Range is the source of much of the surface and groundwater water for both the west and east sides. Groundwater systems within the permeable High Cascades in particular are important components of the system from both ecological and water resources perspectives (Gannett et al., 2001; Jefferson et al., 2006; Jefferson et al., 2010). These groundwater systems operate on the timescale of years to decades and connect the amount and location of snowfall to the spring locations via groundwater-flow paths.

The volcanic landscape of the northwestern United States hosts more than half of the high-volume springs (>3 m^3/s) of the conterminous U.S (Meinzer 1927). Many of these springs originate from the volcanoes of the Cascade Range between Lassen Peak, California, and Mount Rainier, Washington (Meinzer 1927), where annual precipitation can exceed 250 cm/yr (Thorton et al., 2016). In northern California, average flow from these springs fluctuates less than 10-15 % annually (Meinzer 1927). Springs between Medicine Lake Volcano and Lassen Peak (Figure 1) contribute approximately half of the annual average flow to the Pit River (~140 m^3/s), the largest source of water to Lake Shasta, California's largest reservoir (Meinzer 1927; Burns et al., 2017a).

In the Cascade Range, groundwater frequently follows flow-paths connecting volcanic uplands to streams and rivers via laterally extensive, low-viscosity lava-flows (Rose et al., 1996; Gannet et al., 2001; Burns et al., 2017b). Fall River issues forth at springs associated with low-viscosity basaltic lava-flow termini (Burns et al., 2017b). Numerous springs issuing from young volcanic rocks feed the Hat Creek (Rose et al., 1996; Davisson and Rose 1997; Figure 1). Large volume springs outputting from low viscosity lava flows serve as a stable year-round and drought-resistant source of water with spring discharge resiliency dependent on factors including multi-year or decadal climate trends and the configuration of the subsurface geology.

The Northwest Volcanic Aquifer Study Area (NVASA, Curtis et al., 2020) is a U.S. Geological Survey (USGS) effort to understand and quantify regional water resources. The study described herein consists of a local study under NVASA's purview that analyzes geologic

controls on groundwater flow between Medicine Lake Volcano, Lassen Peak and Big Valley Mountain (called the Shasta- Lassen Peak- Medicine Lake Volcano study area, hereafter SLMSA, Figure 1). It focuses on the Hat Creek basin (hereafter the *Focus Area,* Figure 1, Figure 2). In order to understand the hydrogeologic system of the Focus Area, new geologic maps, topographic analysis, Thermal InfraRed (TIR) temperature data, and streamflow data provide new insight into the surface and groundwater system of the Hat Creek basin.

2 Materials and Methods

2.1 Geology and hydrology of the SLMSA

2.1.1 Plate tectonic setting

The SLMSA spans the northwestern section Basin and Range extensional province, the southern end of the Cascades subduction zone and related volcanic arc (the Cascade Range), and the northwestern edge of the Walker Lane Fault Zone (Figure 1a; Blakely et al., 1997; Langenheim et al., 2016). Cascade Range and Basin and Range-style faults interact in the SLMSA (Blakely et al., 1997; Muffler and Clynne 2015). Cascade Range arc and Basin and Range low-volume extensional style volcanism both use N-S and NW-SE striking faults as conduits for magma to flow to the surface (Muffler et al., 2011; Muffler and Clynne 2015). Dextral oblique and normal faults partition crustal deformation in the region; these normal fault-related basins and ranges reflect the dominant structural expression in the regional topography (Unruh et al., 2017; Blakley et al., 1997).

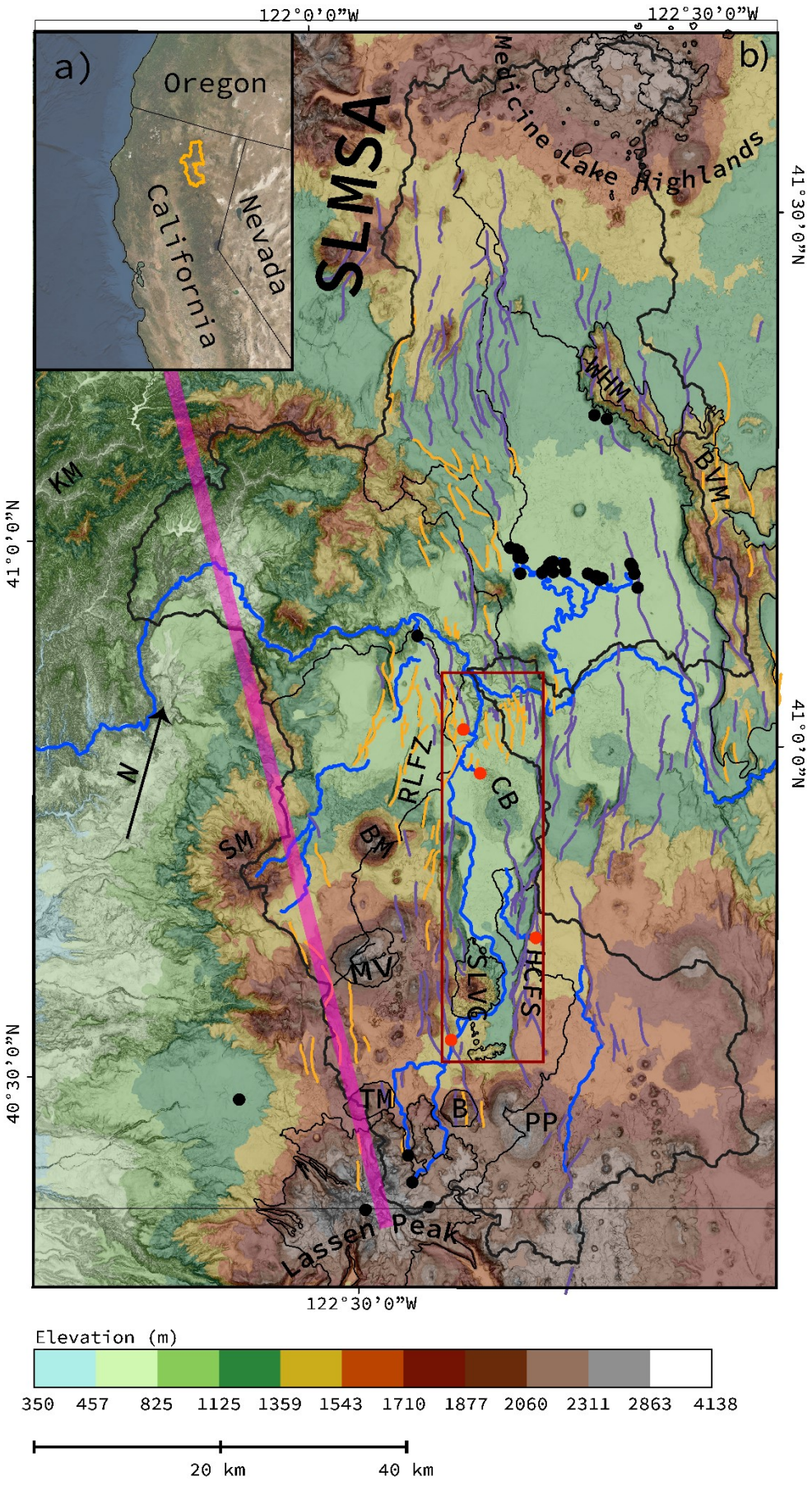
a)
Oregon
California
Nevada
b)
SLMSA
Medicine Lake Highlands
WHM
BVM
KM
N
RLFZ
CB
SM
BM
MV
SLVC
HCFS
TM
B
PP
Lassen Peak
122°0'0"W
122°30'0"W
41°30'0"N
41°0'0"N
40°30'0"N
Elevation (m)
350 457 825 1125 1359 1543 1710 1877 2060 2311 2863 4138
20 km
40 km

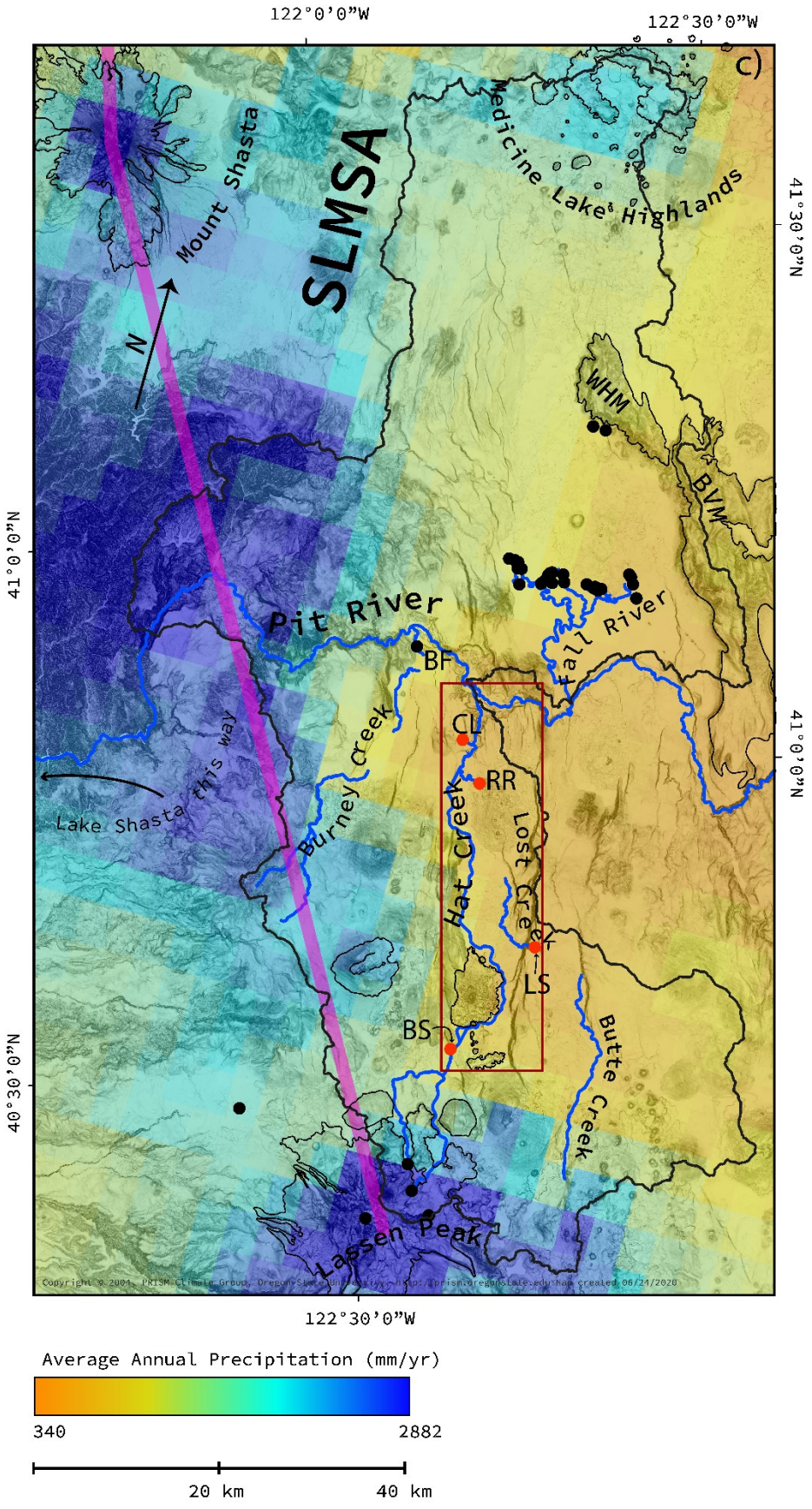
122°0'0"W
122°30'0"W
c)
SLMSA
Mount Shasta
Medicine Lake Highlands
N
WHM
BVM
41°30'0"N
41°0'0"N
40°30'0"N
Pit River
Fall River
BF
CL
RR
LS
BS
Burney Creek
Hat Creek
Lost Creek
Butte Creek
Lake Shasta this way
Lassen Peak
Copyright © 2004 PRISM Climate Group, Oregon State University, http://prism.oregonstate.edu, Map created 06/21/2020
Average Annual Precipitation (mm/yr)
340
2882
20 km
40 km

Figure 1: Location (a), elevation (b), and precipitation (c) maps of Shasta-Lassen-Medicine Lake-Study-Area (SLMSA, yellow in a, grey in b and c) and the Focus Area (brown/red box). a) Location map showing the regional context of the SLMSA. b) Elevation mapped on slope shaded relief includes labels for topographic features, east-dipping and west-dipping faults (orange and blue/purple, respectively), streams and rivers (labeled on Figure c). From south to north topographic features include, PP: Prospect Peak, B: Badger Mountain, TM: Table Mountain, SLVC: Sugarloaf Volcanic Chain with Sugarloaf Peak as the main edifice (Turrin et al,. 2007), MV: Magee Volcano, BM: Burney Mountain, SM: Snow Mountain, CB: Cinder Butte, KM: Klamath Mountains, BVM: Big Valley Mountains, WHM: White Horse Mountain. The labeled faults are the Rocky Ledge Fault Zone (RLFZ), in orange, and the Hat Creek Fault zone (HCFS), mapped in purple. Pink line represents the active arc axis (modified from Wells and McCaffrey 2013). c) Average Annual Precipitation (1981-2010 PRISM) mapped on a slope shade with rivers (blue lines) and large springs (circles). Focus Area springs are in red, labeled spring include BF: Burney falls, whereas labeled Focus Area springs include CL: Crystal Lake Springs, RR: Rising River Springs, LS: Lost Springs and BS: Big Springs. Fall River headwater springs are not individually labeled. Rivers and Creeks include Butte Creek in the southeast, Lost Creek on the east, Hat Creek in the Hat Creek Focus Area box, Burney Creek west of Hat Creek, Fall River to the north and Pit River, flowing east to west across the figure. The highest amounts of precipitation (dark blue) fall on the high elevation Cascade Range (white/grey in a): Lassen Peak to the south, and Mount Shasta (MS). East of the axis of the Cascade Range relatively high precipitation continues at the relative higher elevation peaks such as Medicine Lake Highlands and Prospect Peak. SLMSA does not include the region next to Mount Shasta because water that drains from Mount Shasta to Lake Shasta uses the surface water system via the Sacramento River.

2.1.2 Geographic setting

The SLMSA lies between Medicine Lake Volcano (MLV) to the north, Lassen Peak (LP) to the south and the Big Valley Mountains (BVM) to the east and Mt. Shasta to the west (Figure 1). The Pit River bisects the SLMSA and gains water from the Fall River and Mt. Shasta to the north, and Hat and Burney Creeks to the south, before draining into Lake Shasta to the west (Figure 2b).

2.1.3 Precipitation

The Cascade Range orographic effect causes a rapid decline in average annual precipitation with distance east from the crest of the Cascade Range (Figure 1c). However, Medicine Lake Volcano and other topographic highs east of the crest receive relatively high average annual precipitation (> 100 cm/yr; Figure 1, PRISM).

2.1.4 Previous Work

Most past hydrogeologic studies in SLMSA focused on geochemically identifying potential groundwater recharge locations, sources of groundwater discharge into streams, and hypothetical fluid-flow paths in the Medicine Lake geothermal system. Rose et al., (1996) used groundwater geochemistry of springs in the SLMSA to show that water from springs feeding Lost Creek, Rising River and Crystal Lake flows north from Lassen Peak, whereas water sourced from an elevation similar to Crater Rim on Magee Volcano feeds Big Spring (Figure 1). Burns et al., (2017b) built upon the foundational work of Rose et al. (1996), Davisson and Rose (1997), Manga and Kirchner (2004) and Davisson et al. (2014) to study the relationship between climate, and spring-flow discharge and temperature in Medicine Lake Volcano groundwater system. These studies found that the length of groundwater-flow paths, the vadose zone's ability to thermally insulate and the heat capacity of the aquifer and surrounding geology work together to buffer spring temperatures from rapidly changing surface temperatures.

Previous work may be used to deduce general properties of the SLMSA groundwater/surface water exchange. However, to date, an in-depth analysis of the relationship between structure, stratigraphy and groundwater-flow of the area between Medicine Lake Volcano and Lassen Peak has yet to take place. Generally, both groundwater and surface-water flow from the ring of topographically high, high-precipitation uplands surrounding the SLMSA towards the Pit River (Figure 1). In the morphologically similar upper-Klamath and upper-Deschutes river basins (the two eastside Cascade Range basins immediately to the north of the SLMSA), highly permeable younger volcanic rocks form productive aquifers that often discharge at large springs at structural barriers or where young volcanic rocks onlap older less-permeable rocks (Gannett et al., 2001).

The Pit River originates outside the SLMLSA to the east, though most of the flow delivered to Lake Shasta accumulates from streams within the SLMLSA (Meinzer 1927). Fall River originates from a series of springs that emerge at the toes of lava-flows hydrogeologically linked to lava-flows sourced from the Medicine Lake Volcano highlands before flowing south to the Pit River (Figure 2; Burns et al., 2017b). Hat Creek headwaters are two small springs near Lassen Peak on the northern flank, flowing ~78 km downstream along which, three large spring

complexes (Big Spring, Rising River, and Crystal Lake) contribute to the creek (Figure 1, Figure 2). Isotopic data indicate that water sourced from Lassen Peak and some adjacent volcanic peaks serve as sources for the Hat Creek springs (Rose et al., 1996; Figure 1). Butte Creek and Lost Creek (Figure 1) both originate at springs above Hat Creek (generally within the Hat Creek surface water drainage) and disappear into the aquifer system while flowing over permeable volcanic units Figure 2). Based on position in the landscape, Lost Creek spring might be the reemergence of Butte Creek (Figure 2). Burney Creek begins on Snow Mountain before flowing around Burney Mountain and vanishing into permeable volcanic rock and remerging twice, the final time ~1.5 km upstream of Burney Falls. At Burney Falls large springs flow from volcanic rocks forming the cliff behind the falls (Figure 1c).

2.1.5 Lava-flow viscosity, cooling, and geomorphic form

In the SLMSA, volcanic rocks can be divided into two geochemical groups 1) high-viscosity lava-flows (purple on Figure 2) or 2) low-viscosity lava-flows (green, Figure 2)**.** Low-viscosity lava flows tend to flow laterally, filling valley bottoms, and high-viscosity lava flows form peaks and have limited lateral extent (Lyle, 2000; Manga, 1997; Manga, 2001; Harris 2013). Volcanic units are separated into high- and low-viscosity based on simplified geochemistry and landform (Figure 2c). Calc-alkaline rocks, linked to arc volcanism, form the high-viscosity (purple) peaks; and low-viscosity low-Potassium olivine tholeiites (48–52% SiO_2), associated with crustal extension, form the extensive (green) valley filling lava flows (Clynne and Muffler 2010, Muffler and Clynne 2015, Clynne and Muffler 2017). Multiple eruptive episodes of low-viscosity eruptions created a stratigraphic sequence of stacked lava-flows separated by sedimentary interbeds deposited between volcanic eruptions (Burns et al., 2011).

Cooling forms many of the primary geomorphic features and textures found in high-viscosity and low-viscosity lava-flows. Cooled-falling rubble pushed forward and overridden as the lava-flows, boiling water in soil or degassing of the lava-flow generate the interconnected vesicles and cracks found in lava-flow tops and bottom (Manga, 2001). Lava-flow interiors also display a range of cooling textures but are often dense, possibly with cooling joints (Lyle, 2000).

2.1.6 Hydrogeologic implications of lava-flow viscosity, cooling, and geomorphic form

Geomorphic features, like lava-flow tops (Manga, 2001), and age-related features (Jefferson et al., 2010; Burns et al., 2017b) influence groundwater-flow in volcanic systems. Porous and permeable lava-flow tops, bottoms and interflow zones, where one lava-flow top meets the overlying lava-flow bottom, often serve as the primary horizontal fluid-flow media in volcanic systems (Gannet et al., 2001; Manga, 2001; Burns et al., 2012; Burns et al., 2016). Extensive jointing can, in some cases, serve as a mechanism to explain vertical connection of volcanic aquifers (Davisson et al., 2014; Gingerich, 1999), but cooling joints may not form open-connected fractures or may be filled with alteration minerals, preventing vertical fluid flow (Burns et al., 2016). Alteration increases with age and in hydrothermal systems with temperature and depth (Burns et al,. 2016; Burns et al., 2017a), and permeability decreases with increased alteration (Gannet et al., 2001; Jefferson et al., 2010; Burns et al., 2017a). As volcanic rocks age, weathering creates low permeability soils whereas secondary mineralization fill cracks and pores, both processes reduce porosity and permeability (Gannet et al., 2001; Jefferson et al., 2010; Burns et al., 2017a). A range of authors document the decreasing permeability of volcanic rocks with age (Jefferson et al., 2010), which has been attributed to alteration and plugging of permeable pathways over time (Jefferson et al., 2010; Burns et al,. 2017a; Burns et al,. 2017b). Drainage density, or the length of streams and rivers divided by the area containing them, on volcanic landscapes related to ephemeral streams, streams and rivers serves as a proxy for the alteration, age and permeability of the volcanic rocks (Jefferson et al., 2010). Rubbly, poorly vegetated, high-viscosity and high elevation volcanic peaks with poor surface drainage networks (e.g., Sugarloaf Peak) serve as the primary sources of groundwater recharge. These older rocks often display signs of surface water-flow and erosion (Jefferson et al., 2010). Systems with low dissection maintain their primary volcanic permeability structure, whereas highly dissected reaches no longer retain their primary permeability structures (Jefferson et al., 2010).

2.2 Geology and Hydrology of the Hat Creek Focus Area

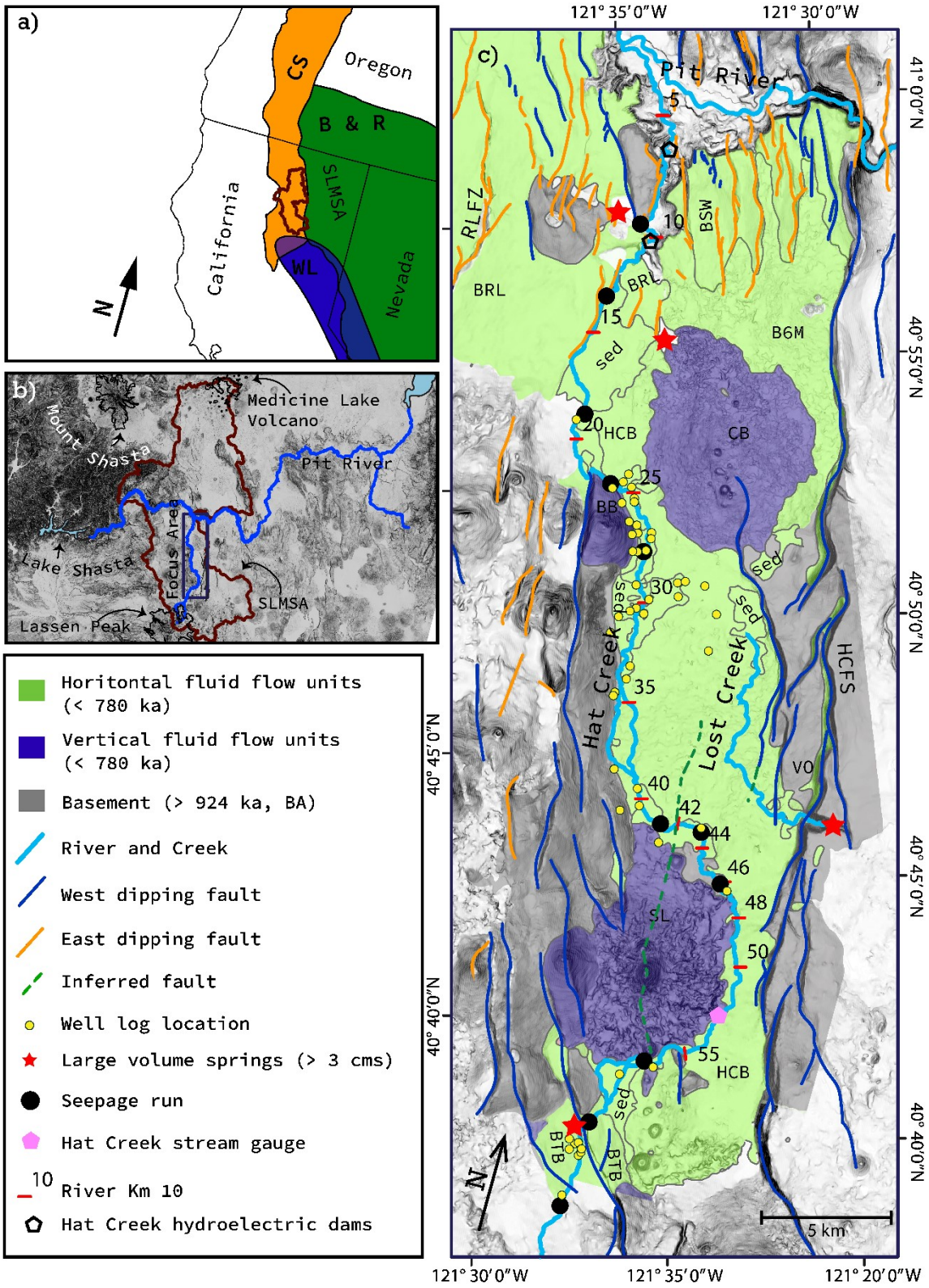

Figure 2: Geology of the Hat Creek Focus area in Context of the western U.S. (a) Geologic setting of the SLMSA in context of western U.S. The Basin and Range extensional province (B&R), Cascade Range (CS), and Walker Lane (WL) intersect in the region of the study area (red/brown outline). Modified from Langenheim et al (2016) and from USGS physiographic divisions of conterminous U.S. (b) Geographic setting of SLMSA and the Pit River basin. Dark blue box indicates the location of the Hat Creek Focus Area (Figure 1c). (c) Hydrogeologic map of the Hat Creek basin. Volcanic rocks grouped into three units: low-viscosity horizontal-fluid-flow units, which also included Holocene sediments (green; individual informal unit names - HCB: Hat Creek Basalt, BRL: basalt of Rocky Ledge, BTB: basalt of Twin Bridges, B6M:basalt west of Six Mile Hill, BSW: basalt of Sam Wolfin Spring, large sediment units: sed), high-viscosity vertical-fluid-flow units (purple; individual informal unit names - BB Brown Butte, CB: Cinder Butte, SL: andesite of Sugarloaf Peak), and older Basement units (grey; BA: volcanic rocks older than924 ka). Informal names of volcanic units based on Clynne and Muffler (2015). Faults colored by dip direction: blue - west-dipping, orange - east dipping (HCFS: Hat Creek Fault System, RLFZ: Rocky Ledge Fault Zone). Fault dip direction established with a lidar derived slope shade map, USGS Active Fault Database (https://pubs.usgs.gov/fs/2004/3033/fs-2004-3033.html), and geologic mapping. Small circles represent locations of well logs, large black circles represent 2019 streamflow measurement sites. Red stars represent large-volume springs. Pink hexagon is the Hat Creek stream gauge. Empty hexagons identify the two Hat Creek run-of-the-river dams.

2.2.1 Geologic Structure

Faulting plays two key roles in the geologic evolution of the Focus Area by 1) determining the shape of the basin and 2) controlling the source and extent of volcanic units deposited within the basin (Leeder and Gawthorpe 1987; Gawthorpe and Leeder 2000). In the Focus Area, the Hat Creek Fault system (HCFS) bounds the valley on the east, providing most of the relief (Blakeslee and Kattenhorn 2013) and controls the geometry of the basin (Langenheim et al., 2016; Figure 2). Crustal-scale faults act as pathways for the vertical migration of magmas (Le Corvec et al., 2013; Muffler and Clynne 2015; Clynne and Muffler 2017) resulting in mapped volcanic centers like Sugar Loaf and Cinder Butte collocated with fault traces.

Previous geologic work suggests two structural models for the Hat Creek basin. In one model, the basin is envisioned as a full graben bounded by the HCFS to the east and the Rocky Ledge Fault zone (RLFZ) and associated faults to the west (Austin 2013; Clynne and Muffler 2017, Figure 1). For the second model, principal evidence favoring half graben geometry includes the basin's asymmetric geometry (Muffler et al., 1994), east-tilting volcanic and volcanoclastic units (Anderson 1940, Kattenhorn et al., 2016), and the eastward thickening of valley fill (Langenheim et al., 2016).

Mapped faults in the Focus Area helps refine the structural models for extension in the Hat Creek basin and the SLMSA at large. On the eastern margin of the basin, the HCFS, a west dipping fault, trends SSE-trending for 47 kms along the eastern margin of the Hat Creek basin and has a maximum vertical displacement of 370 m, and separates the valley bottom from the adjacent uplifted fault-blocks (Figure 1; Anderson 1940; Muffler et al., 1994; Blakeslee and Kattenhorn 2013, Kattenhorn et al., 2016; Langenheim et al., 2016). On the southwestern margin of Hat Creek basin, the hitherto unnamed fault collocated with Big Spring also dips to the west (Figure 2). To the north of Brown Butte, the east dipping RLFZ accommodates strain on the western margin of the basin while the HCFS maintains strain accommodation on the east (Anderson 1940, Austin 2013, Figure 1). From south to north, fault dip changes from predominantly down-to-the-west, (Anderson 1940; Muffler et al., 1994, Langenheim et al., 2016) to mixed east dipping on the west side of the basin and west dipping in the east, respectively (Austin 2013, Figure 1, Figure 2).

2.2.2 Volcanic history

Young-low viscosity flows in the Hat Creek basin covering the valley floor fall, young-high viscosity peaks that rise above the floor, and older volcanic rocks bound the basin on the east and west sides and in the subsurface. The ~800 ka basalt of Twin Bridges is exposed to the southwest of the Focus Area and consists of multiple lava-flows ranging in thickness from tens of centimeters to a few meters (Clynne and Muffler 2010, Figure 2c). Sugarloaf volcano and associated smaller cones align along an inferred fault that trends 345° (Figure 2c) and consist of a series of volcanic andesites and basaltic andesites erupted between 77 (+/- 11 ka) and ~46 (+/- 7 ka) (Clynne and Muffler 2010; Turrin et al., 2007, Figure 2c). Cinder Butte volcano is a basaltic andesite in composition and has a 38±7 ka age (Clynne and Muffler 2017). The Andesite of Brown Butte is a young (<1 Ma) volcano whose exact age is unknown (Figure 2c). Twenty-four ka (+/- 6ka), vents in the southern portion of the Focus Area erupted the Hat Creek Basalt (HCB), multiple low-potassium olivine tholeiitic basalt-flows, and buried sections of the Hat Creek Fault (Turrin et al., 2007, Figure 2c) and the basalt of Twin Bridges in the southwest. The basalt of Rocky Ledge, outcrops in the northern portion of the Focus Area (Clynne and Muffler 2017).

2.2.3 Hydrology

Geochemical analyses of springs were used to determine potential sources for spring water feeding Hat Creek, which enables understanding potential fluid flow paths. Relatively Lower $\delta^{18}O$ values indicate a flow weighted average elevation matching Crater Peak on Magee Volcano (Rose et al., 1996), though they could also represent a range of elevations from Lassen Peak to Badger Mountain (Figure 1). Rising River springs and Crystal Lake springs source water from the high elevation, high precipitation region near Lassen Peak (Figure 1; Rose et al., 1996; Davisson and Rose 1997). Big Spring and Rising River spring both appear in the Hat Creek basin, meaning that fluid flow paths feeding these springs must travel across, around or through the structures responsible for the creation of the basin (Figure 2). Crystal Lake springs appears near the basin rim on the southwest (Figure 2), therefore fluid flow paths feeding it might run closer to Burney Mountain to the west of the Focus Area (Figure 1).

2.3 Data types

The mapped geology, simplified into hydrostratigraphic units, and water well drilling logs translate the conceptual model into a 3-D representation of the Hat Creek groundwater system. Trend surfaces for lava flow tops and bases created using interpreted well-log geologic contacts estimate location of lava-interflows (potential aquifers) in the subsurface. Late-summer streamflow-measurements paired with stream temperature estimates from an airborne TIR survey identify locations and magnitude of stream gains and losses (e.g., stream confluences, springs, etc.). Overlaying gains/losses onto hydrostratigraphy allows identification of geologic controls on groundwater-flow.

2.3.1 Simplified Geologic Maps

Simplified geologic maps, separating volcanic units by age (a surrogate for permeability) and morphology (a surrogate for vertical and horizontal connectivity), were constructed using geologic mapping and age data from L. J. P. Muffler and associates, 1/3 arc second lidar digital elevation models (DEM), and the USGS active faults database (The National Map, accessed March 2019; Figure 2). A DEM-derived slope map, published geologic mapping (Clynne ad Muffler 2010; Figure 2), and data from the USGS Active fault database constrain fault and contact locations. Fault location and extent, strike, dip, and dip direction were modified from the

USGS active faults database (Quaternary faults and folds database, downloaded November 2018) with GIS analysis including aspect and slope maps. Aspect maps derived from lidar data reveal the direction slopes face, and provides the dip direction of faults identified from the DEM. Additional faults were inferred from lidar data using the following rules: 1) long (>800 m) lineaments and with 2) slopes $\geq$ 25° via a 1/3 arc second lidar DEM, where3) shorter (<800 m), younger (15-24 ka) faults have smaller widths (100 m), whereas 4) older (Pleistocene), longer (~ 14 km) faults have wider widths (500 m) (Blakeslee and Kattenhorn, 2013).

2.3.2 Hydrogeologic Units

For the purposes of the hydrogeologic interpretation volcanic units are divided based on age and viscosity/simplified composition and morphology. These subdivisions are young (< 780 ka) volcanoes and lava-flows and basement (BA, >924 ka). The HCFS has a maximum age of 924 ka, representing the maximum age of the Hat Creek basin, which creates the accommodation space that the younger units fill. BA deposits (> 924 ka), serve as the lower boundary of the aquifer (Jefferson et al., 2010, Guffanti et al., 1990). Young volcanic rocks are further subdivided into high lava-flow viscosity (purple unit, Figure 1) and low lava-flow viscosity rocks and Quaternary sedimentary interbeds (green unit, Figure 1). The green low viscosity units have large horizontal extents, host shallow aquifers, and are the horizontal fluid flow unit (Figure 2c). Whereas the basement unit can transport water, the age gap between the basement unit the youngest of the horizontal fluid flow units (< 150 ka) provides the permeability contrast that accentuates the importance of the horizontal fluid flow unit (Jefferson et al., 2010, Burns et al., 2016, Burns et al., 2017b). Mapped purple high viscosity units were lumped together because these units do not have obvious channels along their flanks (Figure 2c). Although purple units likely have flow tops and bottoms and they can move water horizontally, they are not horizontally extensive enough to properly host horizontal aquifers. Purple units are the vertical fluid flow unit (Figure 2c).

2.3.2 Simplified Well Log analysis

Water well logs (Figure 2) were used to estimate the dip of young volcanic units in the subsurface. Picking stratigraphic surfaces allows for construction of a trend surface passing

through picks for each unit bounding surfaces. All well logs received a rating between 0 (no details about stratigraphy) to 3 (stratigraphic horizons and water bearing units are identified along the borehole) based on depth, detail and quality of description. Stratigraphic picks were made using well logs rated 2 and 3. Stratigraphic contact elevation was also estimated from mapped surficial geology. For each horizon, a trend surface was computed using python's least-squares planar fit (Galton, 1886) or RStudio's LOESS smoothing function (Cleveland, 1979). Only the general dip directions and magnitude are used to develop the conceptual hydrogeologic framework, but future efforts include construction of a 3D digital geologic model for the focus area.

2.3.3 Streamflow Measurements

Daily streamflow estimates at the Hat Creek gauge (USGS 11355500, Figure 2c) and late season (September 8-19) 2019 streamflow measurements along Hat Creek (Figure 2c) identify spatial patterns in groundwater discharge along Hat Creek. The 2019 Hat Creek late-summer seepage-run (streamflow measurements collected over the length of a stream for the purposes of estimating groundwater discharge and infiltration) was conducted from September 8-19 (Figure 2; NWIS, https://waterdata.usgs.gov/ca/nwis/rt). Streamflow estimates along Hat Creek from 1912, 1921,1922, 1928, 1988, 2002, 2015, 2016 and 2017 compared with the 2019 seepage-run give an idea of the variability along the reach of the Hat Creek (NWIS, https://waterdata.usgs.gov/nwis). Daily streamflow estimates at USGS Hat Creek stream gauge from the years 1928 – 1930, 1960 –1993 and 2016 – 2019 are used to identify annual streamflow variability in the Hat Creek over a range of years and climate conditions (USGS Current Water Data for California, downloaded October 2019). Assuming evapotranspiration is small (negligible compared to other inflows and outflows), all measured gains and losses from the surface water system come from interaction with groundwater or tributaries.

2.3.4 Airborne Stream Temperature Survey

In 2018, late-season morning (September 25, 7:05-9:22 am) and afternoon (September 24, 4:37-7:00 pm) Thermal InfraRed Aerial Image (TIR) surveys (Torgersen et al., 2001) measured water surface temperature of Hat Creek, allowing examination of temperature variations resulting from atmospheric heating, spring discharge, and addition of water from other

sources (e.g., tributary streams and dams). The morning and afternoon surveys were conducted using a helicopter-mounted using a FLIR system SC6000 TIR sensor flown 400 m above Hat Creek. FLIR system SC6000 sensor measures wavelengths 8-9.2 μm. A supplementary evening flight took place on September 25 from 6:20 to 7:00 pm to capture a section of the river missed during the September 24 evening flight. Fourteen temperature probes distributed along the Hat Creek were used to calibrate the spatially continuous TIR raster datasets. TIR and probe data showed good agreement, with all but two differences between probe and survey falling below 0.6 °C, resulting in only minor adjustment of TIR data during calibration. The two remaining probes were excluded from the calibration process, one due to instrument failure, and the other because it was out of the coverage of the morning flight. Pixels are 0.5 by 0.5 m. To estimate a representative stream temperature, the median temperature was calculated by selecting 10 pixels across the channel sampled at points spaced every 10 meters along the stream length. Riparian vegetation or narrow channel width contribute to a lack of pixels that represent 100% stream surface and therefore create local holes in the data. Local holes (< 600 m) in 10 m data do not affect the continuity of the data, however, larger holes (> 600 m) in the data are visible as data gaps.

2.3.5 Groundwater Temperature Estimation at Springs

Streamflow and TIR temperature measurements immediately upstream and downstream of springs can be used to estimate flow-weighted average groundwater discharge temperature by using conservation of mass and energy. Despite having a name that implies a single discharge location (e.g., Big Spring), spring discharge in this region is often diffuse along a comparatively short stream reach, and spring discharge temperature may vary along the length of the stream. Conservation of energy requires that downstream energy flux of the stream equals the sum of energy flux from upstream plus energy flux from the springs complex.

$$\boldsymbol{\Phi_d = \Phi_s + \Phi_u} \qquad \text{Equation 1}$$

Where Φ, is the energy flux of the flowing water and subscripts d, s and u are downstream, spring and upstream, respectively. Each energy flux can be translated into volumetric-flow and temperature:

$$\Phi = Q * \rho * c * T \qquad \text{Equation 2}$$

Where T is the temperature above absolute zero:

$$T = T_m - T_{zero} \quad \text{Equation 3}$$

Volumetric flux is Q, density of water is ρ , specific heat capacity of water is c, T_{zero} is the temperature of absolute zero and T_m is the measured or estimated temperature (m is an index having values: d, s, or u; depending on the flux represented by equation 2).
Conservation of mass is:

$$\rho_d Q_d = \rho_u Q_u + \rho_s Q_s \quad \text{Equation 4}$$

Assuming density and specific heat capacity are constant, combining equations 1-4, simplifying, and rearranging allows estimation of groundwater temperature from the spring:

$$T_s = \frac{Q_d * T_d - Q_u * T_u}{Q_s} \quad \text{Equation 5}$$

Where Ts is the flow-weighted average temperature of spring discharge.

3 Results

3.1 Stratigraphic Trends

Trend surfaces representing depositional horizons identified as contacts in well logs generally show dipping and unit thickening to the east or northeast. Because trend surfaces vary smoothly in space, both dip direction and dip vary across the modeled trend surface. The uppermost unit (HCB) top forms the valley floor of the Hat Creek basin and is locally buried beneath a thin veneer of Holocene sediments. The HCB thickens to the east-northeast. Both HCB top and HCB bottom both have similar clusters of dip direction (north-north east, northeast) and dips, around 1.2° – 1.4° NE (Table 1). With HCB top defining the top of the HCB unit and HCB bottom defining the bottom, together they can define HCB's potential volume. The upper trend surface for the basalt of Twin Bridges (BTB top) trend surface has dip directions clustered between northeast and east and dips centered on 2.2°, but that vary between 1.4° and 12° (Table 1). Both HCB top and HCB bottom dip to the north rather than the east-north east, as BTB top does. The west-striking, north-dipping slopes of HCB top and HCB bottom both likely reflects that HCB flowed north towards the Pit River (Table 1). BTB tilts to the northeast because it is an older unit that has likely been tilted relatively more than the younger HCB.

Table 1: Strike and Dip values for contacts found from California well logs in Hat Creek valley.

	Max Dip (°)	Min Dip (°)	Med Dip (°)	Max Dip Direction (°)	Min Dip Direction (°)	Med Dip Direction (°)
HCB top	1.30	0.32	1.24	20	351	14
HCB bottom	1.48	1.39	1.43	10	356	357
BTB top	12	1.4	2.17	80	25	62.5

3.2 3D Conceptual Model for the Hat Creek basin

Combining the simplified geologic maps (hydrostratigraphy and structure; Figure 2) with the well-log trend surfaces informs a 3D diagram of the hydrologic system (Figure 3). Brown Butte, Sugarloaf Peak and Cinder Butte and all serve as vertical groundwater-flow rock units (Figure 2c). Horizontal fluid flow units include Hat Creek Basalt, the basalt of Twin Bridges and the basalt of Rocky Ledge (Figure 2c). Basin fill thickens and tilts to the east/northeast (Table 1, Langenheim et al., 2016), illustrating how the geometry of aquifers results in potential connections with Hat Creek (Figure3), dips steepen with age, indicating relatively rapid subsidence on the eastern margin compared to the west of the valley (Figure 3, Table 1). At least two low-viscosity basalt-flows fill the valley (Table 1). Four units are shown schematically to depict how a sequence of units might interact hydrologically (Figure 3). Panel (b) depicts the hypothetical cross section from the incised Lost Creek canyon on the east to the western margin of the Hat Creek basin. Hat Creek flows on the western valley margin by the HCB-Basement contact, resulting in a potential pathway for infiltration to deeper aquifers at the up-dip lava flow margins (Figure 3b). A second cross-section (Figure 3c) illustrates the linkages between the aquifer system and the Hat Creek along the eastern margin of the HCB near the contact with the Sugarloaf lava flows and the subsequent incision through low-viscosity basalts . Large volume springs output at both structural and depositional boundaries (Figure 3), including from the upthrown side of faults (e.g. Lost Creek), at potential fault barriers (e.g., Big Springs), or at the toe of volcanic features (e.g., Rising River).

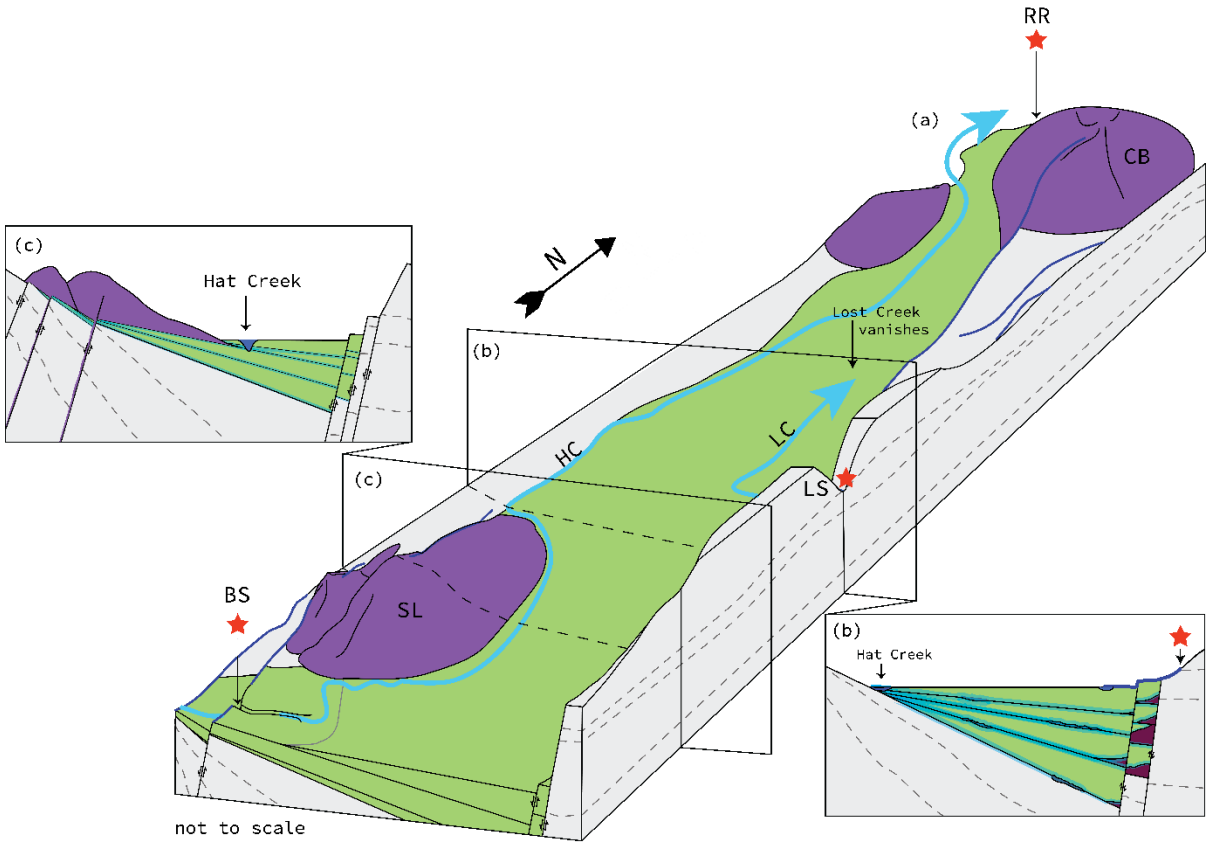

Figure 3: (a) Schematic 3-D diagram of the hydrogeologic organization of the Hat Creek basin. Lateral fluid-flow units are green, vertical-flow units are purple, and no-flow/low-permeability units are grey. West-dipping fault dip direction based on the direction the fault scarp faces at the surface (Figure 2). Hat Creek and Lost Creek in light blue, large-volume spring locations as red stars, labels include BS: Big Spring, LS: Lost Creek, RR: Rising River spring, CL: Crystal Lake spring. (**b**) Schematic cross section cutting across Lost Creek to the north of Sugarloaf Peak. Fluvial and alluvial interbeds in dark red. High-permeability lava-flow tops and bottoms that serve as potential aquifers in light blue. (**c**) Schematic Cross section through Sugarloaf Peak. Schematic 3-D diagram of the hydrogeologic organization of the Hat Creek basin. Stacked laterally connected aquifers are green (horizontal fluid flow units), vertically connected units are purple, and older Basement units are grey. Cross section demonstrates potential pathways to the subsurface (or surface) by way of the purple – green contact or interflow zone. West-dipping fault (dark blue lines) dip directions based on the direction the fault scarp faces at the surface (Figure 2). Hat Creek (HC) and Lost Creek (LC) in light blue, large-volume spring locations as red stars, labels include BS: Big Spring, LS: Lost Creek headwater spring, RR: Rising River headwater spring. (c) Schematic Cross section through Sugarloaf Peak.

3.3 Streamflow and Stream Temperature

Combining streamflow and temperature measurements allows the identification of an alternating pattern of gains (springs) and losses (leakage) along Hat Creek (Figure 4). The late summer 2019 seepage-run measurement locations were selected after considering the 2018 TIR

survey data. Seepage-run data from 2019 and previous years illustrates the general pattern of alternating gaining and losing, but data are sparse, so temperature data is used to more precisely identify stream reaches with groundwater contributions (Figure 4). Prior seepage-run measurements generally follow the 2019 spatial-pattern, indicating that the pattern in robust (Figure 4). The range of late-season streamflow measured at the Hat Creek stream gauge (box and whiskers plot) demonstrates that deviations from the 2019 pattern and are likely due to year-to-year variability in response to droughts or wet periods. Heating or cooling along short stream sections results from springs (e.g., Big Spring) or tributaries (the spring-fed Rising River), allowing the identification of springs complexes (gray bands on Figure 4). One data gap was found near km 14.

3.3 Groundwater Temperature at Springs

Flow-weighted average spring temperature can be estimated for spring complexes using both the morning and afternoon TIR data, if springs are from regional groundwater discharge then the two resulting temperature estimates should agree (Figure 4). Morning and afternoon spring-temperature estimates are compared to each other and with point temperature measurements previously collected (Table 2). Point measurements were likely collected near an obviously large spring or possibly at multiple large springs along the springs complex (e.g., Davisson et al.'s (1997) Rising River measurements are made at different locations as evidenced by the 6 °C difference between the measurements).

Table 2: A comparison of morning and afternoon flow-weighted average spring temperatures estimates with previous measurements.

	Downstream morning Temperature (°C)	Downstream afternoon Temperature (°C)	Upstream morning Temperature (°C)	Upstream afternoon Temperature (°C)	**Estimated morning temperature (°C)**	**Estimated afternoon temperature (°C)**	Temperature (°C) Davisson 1997[1]	Temperature (°C) USGS 2015
Big Springs	7.2	8.9	7.9	15	**7.1**	**8.1**	8,7,7	8.6
Rising River	12.7`[3]	15.7[3]	12.2[3]	17.7[3]	**12.2[3]**	**14.6[3]**	14,8	12.2[2]
Crystal Lake	12.7[4]	13.5[4]	12.2[4]	15.8[4]	**11.6[4]**	**10.8[5]**	10	--[6]

1 Davisson reported temperature to the nearest degree to avoid confusion
2 2019 and 2015 USGS temperature measurement made at the Cassel Road bridge measured 2.3 km from Rising River Springs.
3 TIR temperature survey measurements taken 4.5 km from the RR springs.
4 TIR surveys did not capture Crystal Lake itself, temperature estimates measured over with width of the blue bar from Figure 4.
5 Computed at the focused outflow from Crystal Lake, which is ringed by springs.
6 not recorded.

Big Springs morning and afternoon flow-weighted spring temperature corresponds well to point measurements with all estimates in the range 7-8 °C (Table 2). Flow-weighted estimates of morning and afternoon spring temperature at the Hat Creek/Rising River confluence do not match well because the springs complex is ~4.5 km upstream of the confluence (Table 2). The estimated travel time between Rising River Springs and the confluence with Hat Creek is roughly 2 hours. Assuming a two hour travel time, that the previous night and morning were cooler than the estimated morning temperature (i.e., Rising River cools as it flows from springs to confluence), and the day was warmer than the afternoon estimate (i.e., Rising River heats after spring discharge), then the Rising River springs complex must have a flow-weighted average temperature in the range 12.2-14.6 °C. Rising River morning temperature estimates correspond well to USGS 2015 temperature measurements, which were measured 2.3 km from Rising River springs. Estimated afternoon spring temperatures at Rising River correspond well to the warmer of Davisson et al.'s (1997) measurements (Table 2). Both morning and afternoon estimated Crystal Lake Springs temperatures do not correlate with the single measurement published in 1997 (Table 2, Davisson et al., 1997). Moreover, when selecting temperature estimates for Crystal Lake, a point at the bottom of the temperature drop (blue bar Figure 4) was used at the downstream temperature measurement. Thus, the estimated temperature is likely a flow weighted average of all the springs in the Crystal Lake system between the confluence with Crystal Lake and km 8 (Figure 4).

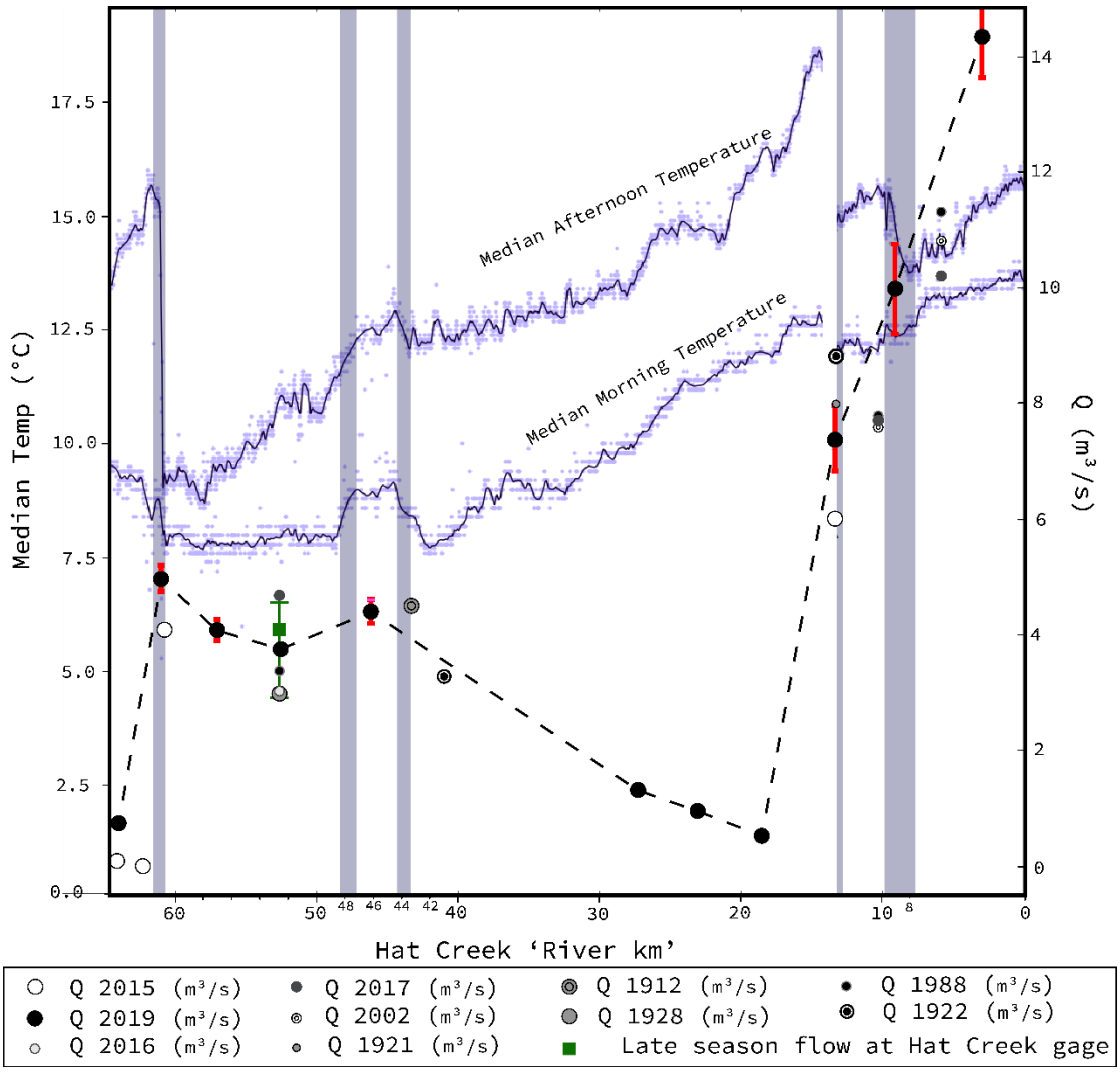

Figure 4: Plot of streamflow (Q in cubic meters per second—m^3/s) and September 24 afternoon and 25 morning 2018 water surface temperature (in °C) along the length of Hat Creek. The dashed black line connects streamflow measurements from the 2019 seepage-run to illustrate the general gaining/losing pattern. All other circular points represent single measurements taken over a variety of years. The ~1 m^3/s flow at river-km 65 is from the watershed above this point, starting with small springs near Lassen Peak (Figure 1). The green square identifies the median minimum August – September temperature taken between years 1928 – 1930, 1960 –1993 and 2016 – 2019 with bar denoting the 10th and 90th percentiles. Light purple dots denote the TIR morning and afternoon temperature values with smoothed fit to emphasize the local trend (dark blue line). Red lines represent errors for the 2019 seepage-run data, which is determined as 5% (fair) or 8% (poor) of the value of measurement on the day of measurement, note that smaller discharges have smaller errors. 2019 values with no visible error simply have errors smaller than the width of the point representing them.

4 Discussion: Patterns in Gains and Losses along Hat Creek

Schematic profiles of geology, creek elevation, streamflow measurements, and stream temperatures along Hat Creek provide a refined and quantitative understanding of the hydrogeology of the Focus Area (Figure 5). Topography, geology along Hat Creek with the higher resolution TIR data identify features that control both gains and losses and locations where the most gains to Hat Creek occur (solid line on Figure 5).

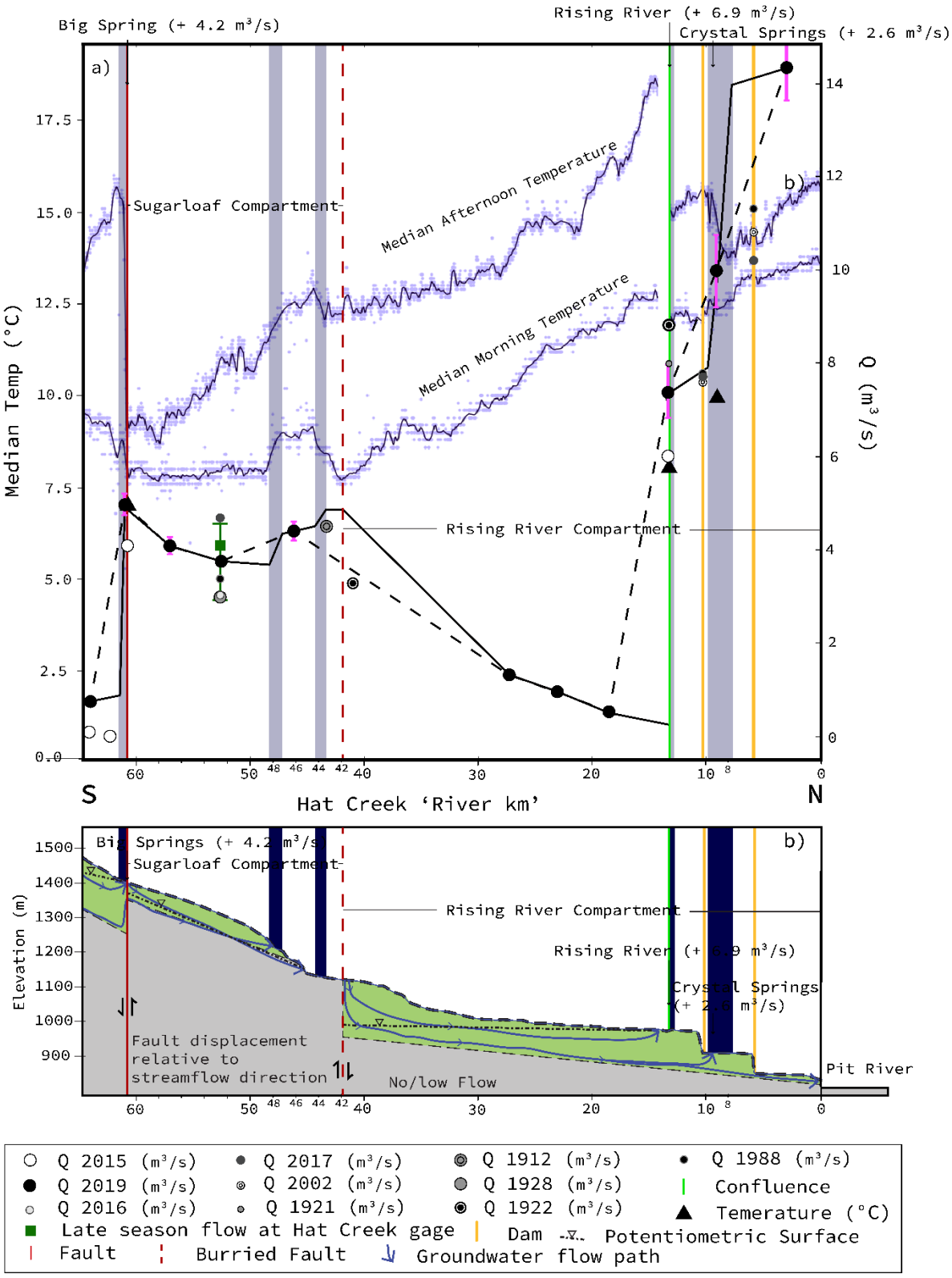

Figure 5: Schematic cross-section (b) along the longitudinal profile of Hat Creek coupled with discharge and temperature measurements (a). Colors and symbols are same as Figures 2 and 3. Transparent blue-grey bands show reaches with large spring complexes and confluences and

depict locations where the most streamflow gains occur on Hat Creek in the black interpreted line. Spring complexes are labeled in (a) with their name and discharges estimated from the 2019 seepage-run. The uppermost aquifer's schematic potentiometric surface is shown as the dashed line with triangle. (b) Hat Creek basin cross-section depicting hydrogeologic units (see Figure 1), faults, springs, and subsurface flow-paths (blue lines arrows indicate flow direction and weather discharging as springs or seeping into the groundwater system). Groundwater-flow barriers separate potentiometric surface, influencing the hydraulic gradient and create conditions for gains or loss to Hat Creek. Faults, or potential groundwater flow barriers, are marked as vertical brown/red lines (solid fault at Big Springs; dashed – buried/inferred fault *north of* Sugarloaf Peak). Circles are sites of stream-flow measurements in 2019. Triangles are point temperature measurements (Davisson and Rose 1996). Spring locations and discharges are labeled in both (a) and (b).

4.1 Compartmentalization of the Aquifer System

Focused groundwater discharge occurs upstream of geologic structures (brown/red lines on Figure 5) resulting in streamflow gains, followed by streamflow losses immediately downstream, indicating the presence of geologic barriers to groundwater-flow. Streams lose when the potentiometric surface for the aquifer in question is lower than the stream, and a path to the groundwater system (e.g. high permeability lava-flow tops and bottoms) is available. Streams gain where both the potentiometric surface for the aquifer is higher than the stream and a pathway to the surface exists. Figure 5b illustrates how barriers result in high potentiometric surface upstream of barriers (groundwater discharge through permeable paths), followed by low potentiometric surface downstream resulting in stream loss through permeable paths (infiltration). A groundwater discharge zone defines the downstream boundary of each compartment, whereas losing stream reaches define the top of the next. The transition from gaining to losing at a known or inferred geologic barrier is used to define two boundaries that define the Focus Area into three lateral hydrogeologic compartments (Figure 5). Hereafter the upstream compartment will be referred to the Big Spring compartment, the middle as the Sugarloaf compartment and the downstream as the Rising River compartment.

4.1.1 Compartment 1: Big Spring compartment

Figure 5 shows only the downstream part of the Big Spring compartment, where TIR data are available. Springs and resulting Hat Creek flow are small upstream of Big Spring (Rose et al., 1996). There are no apparent major groundwater flow barriers between Lassen Peak and Big Spring (Figure 1). The Big Spring fault forces close to 4.2 m^3/s of groundwater into Hat Creek

where Hat Creek travels E-W across a NW-SE trending fault. Uniform and relatively low streamflow from the 2015 and 2019 seepage data indicate that stream temperature above Big Spring responds to atmospheric heating. Between km 62 and 61 at the fault at Big Springs, streamflow increases by a factor of more than 5x (Figure 5a). Rapid cooling of the afternoon stream temperature over a very short stream-length (blue-gray band on Figure 5, Figure 6) shows focused groundwater discharge at Big Spring over a stream length of ~1 km.

Spring water sampled at Big Spring demonstrates a geochemical signature implying multiple elevation sources (Rose et al., 1996). Isotopic composition indicates Big Spring source is consistent with the mixing of water originating across a range of elevations that could including Table Mountain, Badger Mountain, Crater Peak and Lassen Peak (Figure 1, Rose et al., 1996). The estimated cumulative precipitation over these areas/elevations of 7.7 m^3/s is more than sufficient to explain the spring-flow at Big Springs. Hat Creek continues to gain water below the Big Spring compartment and geochemical evidence suggests downstream springs also have a Lassen Peak source (Rose et al., 1996). Therefore, the Big Spring compartment is leaky, or there are alternate groundwater flow paths from Lassen Peak around the compartment, or both processes occur.

4.1.2 Compartment 2: Sugarloaf compartment

The Sugarloaf compartment extends from the fault at Big Spring to near km 42 at an unnamed fault north of Sugarloaf volcano (Figure 6). The Sugarloaf section of Hat Creek loses over the upper two-thirds of the reach and gains over the downstream third, where a groundwater-flow barrier likely exists (possibly the unnamed fault). Again, stream temperature changes over short distances above the fault allow identification of localized groundwater discharge. Modest temperature gains with distance in the afternoon likely represent stream heating due to atmospheric exchange in the upstream reaches (Figure 5a). Until km 48, Hat Creek flows near or over HCB margins resulting in a potential pathway for infiltration to the groundwater system and surface water loss. Groundwater flow to springs may come from two different sources, one warmer (heating of both morning and afternoon stream temperatures near 48 km; blue bar on Figure 5) and one colder (cooling at ~ km 43;blue bar on Figure 5). The groundwater flow barrier at the bottom of the Sugarloaf compartment can be inferred from the change in morning and afternoon temperature estimates trends (~ km 42) and the pattern of

stream gain followed by stream loss (Figure 5, Figure 6).The basement outcrop between km 46 and 44 (Figure 2) and the alignment of the Sugarloaf chain to the west of it near km 41, both indicate that the barrier might be a fault (Figure 6).

Streamflow losses upstream approximately balance downstream gains for the Sugarloaf compartment (Figure 5) implying that this compartment does not need water from outside the basin to explain the water budget. Nearby groundwater-recharge sources include Magee Volcano, Table Mountain and Badger Mountain (Figure 1) indicate that excess groundwater that might be leaking through or past the downstream groundwater-flow barrier into the next compartment. Leakage into a groundwater flow system on the eastside of the Hat Creek valley bottom would help explain the flow rate and geochemistry of the large headwater springs of Rising River.

4.1.3 Compartment 3: Rising River compartment

The Rising River compartment begins with the fault associated with Sugarloaf volcano and ends at the Pit River. Most of the groundwater discharges at depositional contacts (e.g. Rising River headwater springs) and at topographically controlled groundwater outfalls (right-hand side of lower Figure 5). The Rising River compartment loses streamflow in its upstream sections and gains in the downstream sections due to additions from natural sources. Two run-of-the-river dams at the compartment's end (Figure 5) are unlikely to affect streamflow. Hat Creek loses close to 4.5 m^3/s of streamflow between the inferred fault at the top of the compartment (km 42) and the confluence with Rising River (Km 14), and these low-flow reaches heat steadily due to atmospheric exchange and solar incidence (Figures 5 and 6). It is postulated that much of the 4.5 m^3/s of lost Hat Creek flow returns via Rising River headwater springs at the toe of Cinder Butte. However Rising River (6.9 m^3/s) adds an additional >2 m^3/s of streamflow to Hat Creek than the losses in the upstream section of the compartment (Figure 5). The >2 m^3/s of excess streamflow likely reflects water added to the system by Lost Creek, which vanishes in the upper reaches of the Rising River compartment (Figure 6). Losses in the Rising River compartment can be linked to the fault at the top of the compartment, which causes the drop in the potentiometric surface, downstream of which Hat Creek travels along the depositional margin of the HCB (Figure 3b), creating the pathway for losses to the volcanic aquifers. Rising River springs could have additional sources of groundwater flowing through the

eastside of the Hat Creek valley with sources ranging from Lost Creek, Lassen Peak, or the uplands to the east. At the confluence with Crystal Lake springs, Hat Creek gains an immediate 2.6 m^3/s, bringing the total volumetric-flow of HC up to 10 m^3/s. A dam release, or a high volume of water of a different temperature to the creek, would result in a step change in temperature similar to the change at the Rising River confluence. We assume that the distributed springs associated with Crystal Lake adds relatively small volumes of water along the stretch of river between 8-10 km (blue bar Figure 5) ultimately cause the steady decline in temperature north of Crystal Lake springs. The distributed seepage along Hat Creek suggests that most of the 14 m^3/s measured before Hat Creek enters Pit River before km 7 (Figure 5b) from the Crystal Lake springs complex.

Isotopic compositions at Rising River and Crystal Lake springs imply a Lassen Peak source (Rose et al., 1996), but groundwater-flow paths from Lassen Peak might differ, with one flowing down the Hat Creek basin while others might flow down valleys to the west (by Burney Mountain) or east.

4.2 Stream temperatures

Spring temperature estimates using conservation of mass methods are most effective when applied to Big Spring. Rising River springs and Crystal Lake springs, in contrast, have upstream, downstream and spring sections that are difficult to identify, have springs far from Hat Creek or both, which makes groundwater temperatures problematic to estimate. Estimated groundwater temperatures of 8.1 °C (afternoon) and 7.1 °C (morning) at Big Spring are the coolest temperatures estimated for the aquifers feeding Hat Creek. Both temperature estimates do not vary far from the measured spring temperatures of 8°C and 7 °C (Rose et al., 1996;Table 2). Estimated Rising River Spring temperatures are 14.6 °C (afternoon) and 12.2 °C (morning). Whereas the afternoon temperature correlates with the 14 °C temperature measurement (Davisson et al., 1997) and the morning estimate correlates well with the USGS 2015 measurement of 12.2 °C (Table 2), the measurements do not correlate with each other. Davisson et al., (1997) measured Rising River springs itself, whereas the 2018 TIR survey estimates and the USGS 2015 temperature estimates correspond to 4.5 and 2.4 km from Rising River Springs respectively. Max temperatures on September 24, 2018 were 26.7 °C (US Climate data 2020, accessed October 2020). Afternoon temperature estimates calculated 4.5 km away from Rising

River Springs, flowed an estimated 2 hours during the hottest part of the day before reaching Hat Creek. The water measured for the TIR temperature estimates, used to estimate spring temperature, likely underwent atmospheric heating and indicate that Rising River Springs is cooler than the estimated afternoon spring temperature. Crystal Lake Springs had temperature estimates of 11.6 °C (morning) and 10.8 °C (afternoon). Crystal Lake spring morning temperature estimates correlate with Davisson et al., (1997), but afternoon estimates do not (Table 2). TIR derived groundwater temperature estimates do not capture the temperature of Crystal Lake and instead quantify the temperature change that occurs over the 2 km north of Hat Creek river km 10 (blue bars figure 5).

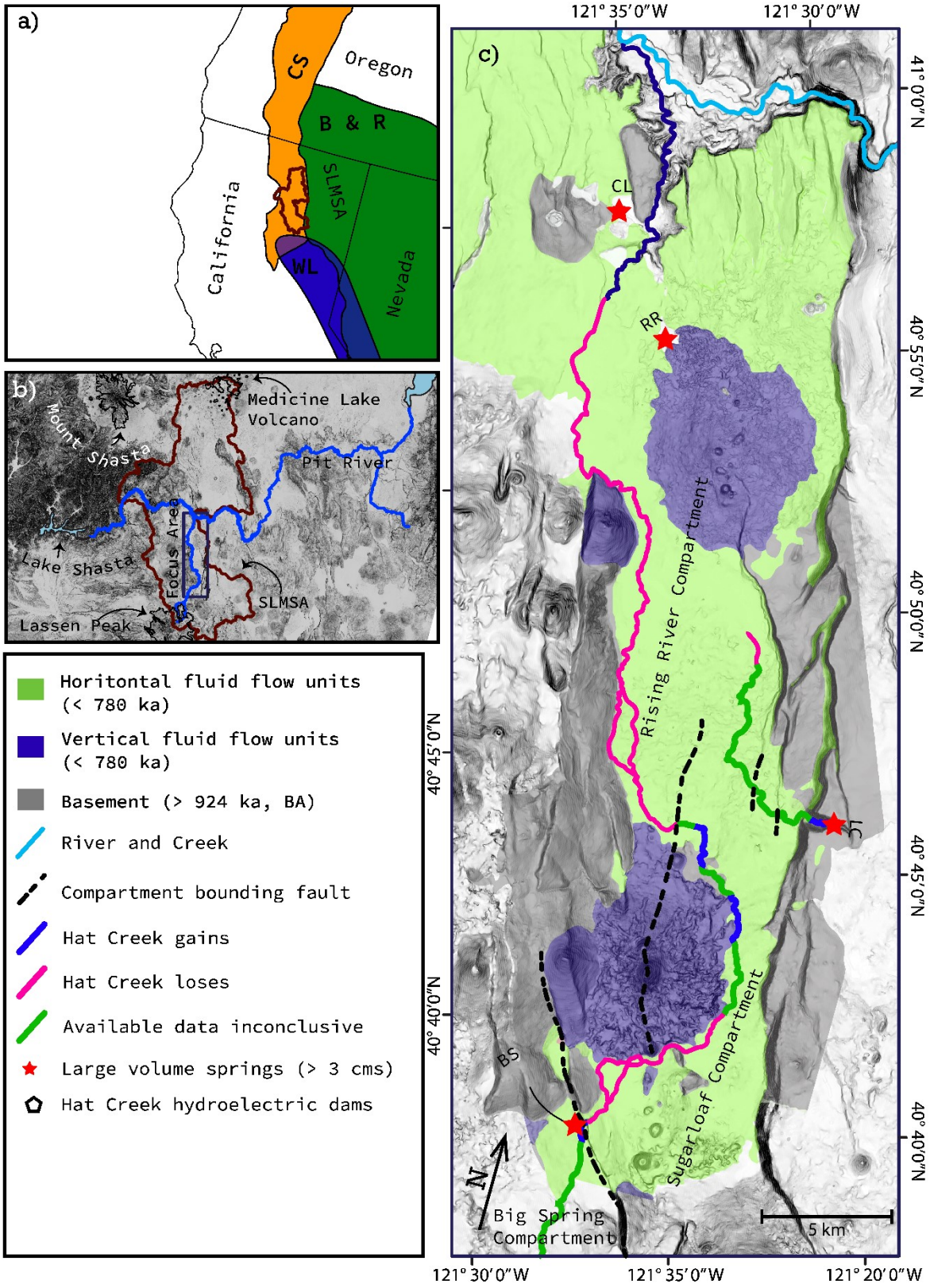

Figure 6: Focus Area with gains (dark blue), loses (pink). Again, the labeled springs are BS: Big Springs, LC: Lost Springs, RR: Rising River Springs, CL: Crystal Lake Springs. Compartments

(Big Spring, Sugarloaf and Rising River) are labeled and the faults that bound them are depicted dashed in black, all dashed faults dip to the west. Dark blue, gaining section occur on the upstream section of each barrier, pink, losing sections occur downstream of each barrier. Lost Creek displays the same trends in gains and loss that Hat Creek does, however gains occur in the very upstream and losses occur at the downstream end gains or losses in the middle of Lost Creek remain unconstrained (Green).

5 Conclusions

Hat Creek flows over a leaky compartmentalized aquifer system with at least three distinct segments separated by geologic structures. The two downstream compartments are characterized by losing stream reaches upstream and gaining downstream. The pattern of streamflow gain followed by streamflow loss generally occurs across structural boundaries created by faults. The upstream most Big Spring compartment gains 4.2 m^3/s at its downstream boundary, the fault at Big Spring. The Sugarloaf compartment begins at the fault at Big Spring and ends at near km 42, at the inferred fault north of Sugarloaf Peak, and gains streamflow lost in its upstream reaches. The downstream most compartment, the Rising River compartment begins at km 42 and ends at Hat Creek's confluence with Pit River. In the Rising River compartment Hat Creek loses almost all its streamflow in its upstream reach but gains close to 14 m^3/s in the km between 14 and 8.

The SLMSA has a similar geologic history to the Hat Creek basin characterized by contemporaneous faulting and volcanism. Streamflow in the SLMSA likely alternates between gaining and losing based in its relationship to local structure. From the lidar, Burney Creek flows next to the first of two east dipping fault systems and disappears before reappearing and disappearing near the second. Butte Creek, in the southeast, appears in the middle of a west-dipping fault, flows across lava plains and disappears as it crosses another fault system east of HCFS. Lost Creek, which crosses the HCFS appears in the downstream section of the sugarloaf compartment and disappears in the upstream section of the Rising River compartment. In theory, all three of these creeks follow the streamflow patters of gains and loss described in the Hat Creek basin.

6 Sources

Anderson, C. A. "Hat Creek Lava Flow." American Journal of Science 238.7 (1940): 477-92. Web.

Austin, L.J. “Evolution of Regional Stress State based on Faulting and Folding near the Pit River, Shasta County, California,” Master’s Thesis, University of Oregon, 2013.

Blakeslee, M.W., Kattenhorn, S.A., “Revised earthquake hazard of the Hat Creek fault, northern California: A case example of a normal fault dissecting variable-age basaltic lavas.” Geosphere, v. 9, (2013): p. 1–13.

Blakely, R.J., L. Christiansen;, M. Guffanti , R.E. Wells, J.M. Donnelly-Nolan, L. J. P. Muffler, M.A. Clynne, J.G. Smith. “Gravity Anomalies, Quaternary Vents, and Quaternary Faults in the Southern Cascade Range, Oregon and California: Implications for Arc and Backarc Evolution.” Journal of Geophysical Research: Solid Earth, vol. 102, no. B10, (1997): pp. 22513–22527.

Burns, E. R., D. S. Morgan, R. S. Peavler and S. C. Kahle. “Three-dimensional Model of the Geologic Framework for the Columbia Plateau Regional Aquifer System, Idaho, Oregon, and Washington.” Reston, Va.: U.S. Dept. of the Interior, U.S. Geological Survey, (2011): Scientific Investigations Report; 2010-5246.

Burns, E.R., Morgan, D.S., Lee, K.K., Haynes, J.V., and Conlon, T.D. “Evaluation of long-term water-level declines in basalt aquifers near Mosier, Oregon: U.S.” Geological Survey Scientific Investigations Report 2012–5002, 134 (2012).

Burns, E.R., Williams, C.F., Tolan, T., and Kaven, J.O. “Are the Columbia River Basalts, Columbia Plateau, Oregon and Washington, USA, a Viable Geothermal Target? A Preliminary Analysis, PROCEEDINGS”, v41, Forty-first Workshop on Geothermal Reservoir Engineering Stanford University, Stanford, California, February 22-24, (2016).

Burns, E. R., M.W. Gannet, D.R. Sherrod, M.K. Keith, J.A. Curtis, J.R. Bartolino, J.A. Engot, B.P. Scandella, M.A. Stern and A.L. Flint. “Geothermal Implications of a Refined Composition-Age Geologic Map for the Volcanic Terrains of Southeast Oregon, Northeast California, and Southwest Idaho, USA.” GRC Transactions, vol. 41, (2017).

Burns, E. R., Y. Zho, H. Zhan, M. Manga, C. F. Williams, S. E. Ingebritsen and J. B. Dunham. "Thermal Effect of Climate Change on Groundwater-fed Ecosystems." Water Resources Research 53.4 (2017): 3341-351.

Cleveland, W.S, “Robust Locally Weighted Regression and Smoothing Scatterplots.” Journal of the American Statistical Association 74:829-836, (1979).

Clynne, M.A., and Muffler, L.J.P., Geologic map of Lassen Volcanic National Park and vicinity, California: U.S. Geological Survey Scientific Investigations Map 2899, scale 1:50,000, (2010).

Clynne, M.A., and L.J.P., Muffler, “Geologic field-trip guide to the Lassen segment of the Cascades Arc, northern California: U.S.” Geological Survey Scientific Investigations Report 2017–5022–K2, 65 p., https://doi.org/10.3133/sir20175022K2. (2017).

Curtis, J. A., Burns, E. R., and R. Sando, "Regional Patterns in Hydrologic Response, a New Three-component Metric for Hydrograph Analysis and Implications for Ecohydrology,

Northwest Volcanic Aquifer Study Area, USA." *Journal of Hydrology. Regional Studies* 30 (2020): 100698. Web.

Davisson, M. L. and P. Rose, "Comparative Isotope Hydrology Study of Groundwater Sources and Transport in the Three Cascade Volcanoes of Northern California." Lawrence Livermore National Laboratory, (1997).

Davisson, M. L. and T.P. Rose, "Recharge and Flow in the Medicine Lake Volcano-Fall Rivers Springs Groundwater Basin, California." Environmental Forensics, vol 15, no 1, (2014): pp. 66-77.

Galton, F. "Regression Towards Mediocrity in Hereditary Stature," Journal of the Anthropological Institute, 15:246-263 (1886).

Gannett, M.W., Lite, Jr., K.E., Morgan, D.S., and Collins, C.A. "Ground-water hydrology of the upper Deschutes Basin, Oregon: U.S." Geological Survey Water-Resources Investigations Report 00-4162, 74 p. (2001).

Gawthorpe R. L. and M. R. Leeder, "Tectono-sedimentary evolution of active extensional basins." Basin Research, vol. 12 (2000): pp. 195-218.

Gingerich, S. B., "Ground-Water Occurrence and Contribution to Streamflow, Northeast Maui, Hawaii." USGS Water-Resources Investigations Report 99-4090, (1999).

Guffanti, M., Clynne, M. A., Smith, J. G., Muffler, L. J. P, and T. D. Bullen. "Late Cenozoic Volcanism, Subduction, and Extension in the Lassen Region of California, Southern Cascade Range." *Journal of Geophysical Research: Solid Earth* 95.B12 (1990): 19453-9464. Web.Jefferson, A., G. Grant, and T. Rose. "Influence of Volcanic History on Groundwater Patterns on the West Slope of the Oregon High Cascades." Water Resources Research 42.12 (2006): N/a. Web.

Jefferson, A., G.E. Grant, S.L. Lewis, and S.T. Lancaster. "Coevolution of Hydrology and Topography on a Basalt Landscape in the Oregon Cascade Range, USA." Earth Surface Processes and Landforms 35.7 (2010): 803-16. Web.

Kattenhorn, S. A., B. Krantz, E. L. Walker, M. W. Blakeslee. "Evolution of the Hat Creek fault system, northern California" in B. Krantz, C. Ormand, and B. Freeman, eds., 3-D structural interpretation: Earth, mind, and machine: AAPG Memoir 111 (2016): p. 121–154.

Langenheim, V., R. Jachens, L. J.P Muffler, and M. A. Clynne. "Implications for the structure of the Hat Creek fault and transfer of right-lateral shear from the Walker Lane north of Lassen Peak, northern California, from gravity and magnetic data: Geosphere." v. 12, no. 3 (2016): p. 790-808.

Le Corvec, N. et al., "Spatial distribution and alignment of volcanic centers: Clues to the formation of monogenetic volcanic fields." Earth-Science Reviews, vol. 24 (2013): pp. 96-114.

Leeder, M. R. and R. L. Gawthorpe, “Sedimentary models for extensional tilt-block/half graben basins.” Tectonics, Geological Society Special Publications No. 28, (1987): pp. 139-152.

Lyle, P. “The eruption environment of multi-tiered columnar basalt flows.” Journal of the Geological Society, London, vol 157(2000): pp.715-722.

Manga, M. "A Model for Discharge in Spring-dominated Streams and Implications for the Transmissivity and Recharge of Quaternary Volcanics in the Oregon Cascades." Water Resources Research, Washington, DC 33.8 (1997): 1813-822. Web.

Manga, M. “Using springs to study groundwater flow and active geologic processes.” Annual Review of Earth and Planetary Sciences, vol. 29, no. 1, (2001): pp. 201–228.

Manga, M., and J. W. Kirchner. "Interpreting the Temperature of Water at Cold Springs and the Importance of Gravitational Potential Energy." *Water Resources Research* 40.5: Water Resources Research, 2004-05, (2004) Vol.40 (5).

Meinzer, O. E. “Large Springs in the United States.” USGS Water-Supply Paper 557, 1927.

Muffler, L.J. Patrick, M.A. Clynne and D.E. Champion. “Late Quaternary Normal Faulting of the Hat Creek Basalt, Northern California.” Geological Society of America. Geological Society of America Bulletin, vol. 106, no. 2, (1994) p. 195.

Muffler, L.J. P., M.A. Clynne, A.T. Calvert, and D.E. Champion. ”Diverse, discrete mantle-derived batches of basalt erupted along a short normal fault zone: the Poison Lake chain, southernmost Cascades” Geological Society of America Bulletin, v. 123, no. 11/12 (2011): p. 2177–2200.

PRISM Climate Group, Oregon State University, http://prism.oregonstate.edu, created 4 Feb 2004.

Rose, T. P, M. L. Davisson, and R. E Criss. "Isotope Hydrology of Voluminous Cold Springs in Fractured Rock from an Active Volcanic Region, Northeastern California." Journal of Hydrology 179.1-4 (1996): 207-36. Web.

Thornton, P.E., M.M. Thornton, B.W. Mayer, Y. Wei, R. Devarakonda, R.S. Vose, and R.B. Cook. Daymet: Daily Surface Weather Data on a 1-km Grid for North America, Version 3. ORNL DAAC, Oak Ridge, Tennessee, USA. (2016): https://doi.org/10.3334/ORNLDAAC/1328

Torgersen, C. E., Russell N. Faux, B. A McIntosh, N. J. Poage, and D. J. Norton. "Airborne Thermal Remote Sensing for Water Temperature Assessment in Rivers and Streams." Remote Sensing of Environment 76.3 (2001): 386-98. Web.

Turrin, B.D., L.J. P. Muffler, M.A. Clynne, D.E. Champion. “Robust 24 ± 6 Ka $^{40}Ar/^{39}Ar$ Age of a Low-Potassium Tholeiitic Basalt in the Lassen Region of NE California.” Quaternary Research, vol. 68, no. 1, (2007): pp. 96–110.

Unruh, J., and J. Humphrey. "Seismogenic Deformation between the Sierran Microplate and Oregon Coast Block, California, USA." Geology 45.5 (2017): 415-418. Web.

U.S. Geological Survey and California Geological Survey, Quaternary fault and fold database for the United States, accessed November, 2018, at: https://www.usgs.gov/natural-hazards/earthquake-hazards/faults.

U.S Geological Survey and California Geological Survey, USGS Current Water Data for California, accessed October, 2019, at: https://waterdata.usgs.gov/ca/nwis/rt.

U.S. Geological Survey, USGS NED 1/3 arc-second n42w122 1 x 1 degree ArcGrid 2019, raster digital data, Reston, VA, https://nationalmap.gov/elevation.html, accessed March 2019.

Wells, R. E., and R. McCaffrey "Steady Rotation of the Cascade Arc.(Author Abstract)." Geology 41.9 (2013): 1027-1030. Web.

Your Weather Service, US Climate Data 2020, https://www.usclimatedata.com/climate/cassel/california/united-states/usca2159, accessed October 2020.